Volume 1 | Number 1 | Jan 2013 | Pages 1–100

Catalysis
Science &
Technology

www.rsc.org/catalysis

ROYAL SOCIETY OF CHEMISTRY

ROYAL SOCIETY OF CHEMISTRY

www.rsc.org/catalysis

Catalysis Science & Technology

COMMUNICATION

Photocatalytic production of hydrogen peroxide from water and dioxygen using cyano-bridged polynuclear transition metal complexes as water oxidation catalysts†

Yusuke Isaka,[a] Kohei Oyama,[a] Yusuke Yamada,[*,b] Tomoyoshi Suenobu[a] and Shunichi Fukuzumi[*,a,c,d]

Hydrogen peroxide was produced efficiently from water and dioxygen using [Ru^{II}(Me$_2$phen)$_3$]$^{2+}$ (Me$_2$phen = 4,7-dimethyl-1,10-phenanthroline) as a photocatalyst and cyano-bridged polynuclear transition metal complexes composed of Fe and Co as water oxidation catalysts in the presence of Sc^{3+} in water under visible light irradiation.

Hydrogen peroxide (H$_2$O$_2$) has merited increasing attention as an ideal energy carrier alternative to hydrogen, because an aqueous solution of H$_2$O$_2$ instead of gaseous hydrogen can be used as an fuel in a one-compartment fuel cell to generate electricity.[1-14] The maximum output potential of an H$_2$O$_2$ fuel cell theoretically achievable is 1.09 V which is comparable to that of a hydrogen fuel cell (1.23 V).[1-14] Thus, H$_2$O$_2$ production from water (H$_2$O) and dioxygen (O$_2$) using solar energy provides an ideally sustainable solar fuel in combination with power generation with an H$_2$O$_2$ fuel cell.[15-17] It is highly desired to improve the catalytic activity for the phtoocatalytic production of H$_2$O$_2$ from H$_2$O and O$_2$ ($\Delta G° = 210$ kJ mol^{-1}, eqn (1)) using earth-abundant metal catalysts.[15-17]
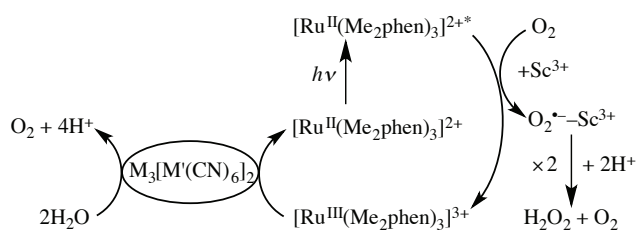
$$2H_2O \ + \ O_2 \ \rightarrow \ 2H_2O_2 \qquad \Delta G° = 210 \text{ kJ mol}^{-1} \qquad (1)$$

We report herein photocataltyic production of H$_2$O$_2$ from H$_2$O and O$_2$ using [Ru^{II}(Me$_2$phen)$_3$]$^{2+}$ (Me$_2$phen = 4,7-dimethyl-1,10-phenanthroline) as a photocatalyst and structurally-definable and molecularly-ordered metal complexes, i.e., cyano-bridged polynuclear transition metal complexes composed of Fe and Co as water oxidation catalysts (WOCs) in the presence of Sc^{3+} in water under visible light irradiation. Among various metal complex-based WOCs, metal complexes were found to play in some cases the role of precursor of actual WOCs.[18,19] In contrast, the cyano-bridged polynuclear transition metal complexes as they are have proven to maintain absolutely high catalytic reactivity with high yield and quantum efficiency for water oxidation.[20]

The photocatalytic cycle is shown in Scheme 1, where the excited state of [Ru^{II}(Me$_2$phen)$_3$]$^{2+}$ is oxidatively quenched by electron transfer to O$_2$ to produce [Ru^{III}(Me$_2$phen)$_3$]$^{3+}$ and the O$_2$$^{•-}$–Sc^{3+} complex, which undergoes the disproportionation in the presence of H$^+$ to yield H$_2$O$_2$.[15,17] Water is oxidised by [Ru^{III}(Me$_2$phen)$_3$]$^{3+}$ in the presence of a heteropolynuclear cyanide metal complex as a WOC to produce O$_2$.

Heteropolynuclear cyanide complexes take a cubic structure provided that contained metal ions allow octahedral coordination.[21,22] Both C and N atoms of cyanide interact with metal ions. When the number of N-bound metal ions is larger than that of C-bound metal ions, the N-bound metal ions need external ligands such as an aqua ligand to fulfil octahedral coordination.[23,24] The number of external ligands can be controlled by considering charge compensation in a heteropolynuclear complex.[23,24] Thus, heteropolynuclear cyanide complexes composed of different metal ions can be designable heterogeneous catalysts for water oxidation.

[a.] Department of Material and Life Science, Graduate School of Engineering, Osaka University, ALCA and SENTAN, Japan Science and Technology Agency (JST), Suita, Osaka 565-0871, Japan, E-mail: fukuzumi@chem.eng.osaka-u.ac.jp
[b.] Department of Applied Chemistry and Bioengineering, Graduate School of Engineering, Osaka City University, Osaka 558-0022, Japan
[c.] Department of Chemistry and Nano Science, Ewha Womans University, Seoul 120-750, Korea
[d.] Faculty of Science and Technology, Meijo University, ALCA and SENTAN, Japan Science and Technology Agency (JST), Nagoya, Aichi 468-8502, Japan
† Electronic Supplementary Information (ESI) available: Experimental section, X-ray diffraction patterns (Fig. S1 and S10b), X-ray fluorescence data (Table S1), DLS data (Fig. S2 and S10c), IR spectra (Fig. S3 and S10a), time courses of H$_2$O$_2$ production under various conditions (Figs. S4, S7, S8, and S9), time courses of O$_2$ evolution amount (Fig. S5 and S6) and estimation of the amount of evolved O$_2$. See DOI: 10.1039/b000000x/
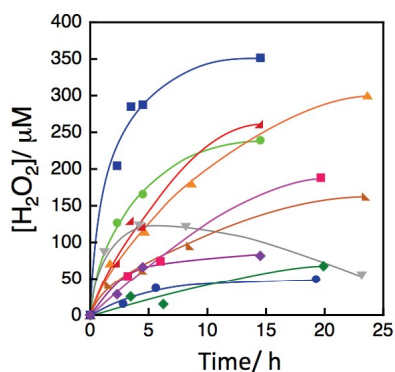
Scheme 1 Catalytic cycle for photocatalytic production of H$_2$O$_2$ from H$_2$O and O$_2$ using [Ru^{II}(Me$_2$phen)$_3$]$^{2+}$ as a photocatalyst and heteropolynuclear cyanide complexes (M$_3$[M'(CN)$_6$]$_2$: M, M' = different metals) as water oxidation catalysts.

Fig. 1 Time courses of production of H_2O_2 from H_2O and O_2 in an O_2-saturated aqueous solution (2.0 mL) of $[Ru(Me_2phen)_3]^{2+}$ (100 μM), $Sc(NO_3)_3$ (100 mM) and a heteropolynuclear cyanide metal complex (1.0 mg) under photoirradiation of visible light ($\lambda > 420$ nm) with a Xenon lamp using a UV light cut filter at room temperature. The employed heteropolynuclear cyanide complexes are $Fe_3[Co(CN)_6]_2$ (blue square), $Co_3[Co(CN)_6]_2$ (red right triangle), $Cu_3[Co(CN)_6]_2$ (green diamond), $Co[Ni(CN)_4]$ (orange regular triangle), $Fe_3[Cr(CN)_6]_2$ (grey inverse triangle), $Mn_3[Fe(CN)_6]_2$ (dark orange right triangle), $Co_3[Mn(CN)_6]_2$ (pink square), $Co_3[Fe(CN)_6]_2$ (light green circle), $Co[Pd(CN)_4]$ (blue circle) and $Co[Pt(CN)_4]$ (purple diamond).

A series of heteropolynuclear cyanide metal complexes containing different metal ions, $Co_3[Fe(CN)_6]_2$, $Co_3[Co(CN)_6]_2$, $Cu_3[Co(CN)_6]_2$, $Co[Ni(CN)_4]$, $Fe_3[Cr(CN)_6]_2$, $Mn_3[Fe(CN)_6]_2$, $Co_3[Mn(CN)_6]_2$, $Co_3[Fe(CN)_6]_2$, $Co[Pd(CN)_4]$ and $Co[Pt(CN)_4]$ were prepared according to the literature.[20] Fig. 1 shows time profiles of production of H_2O_2 from H_2O and O_2 in an aqueous solution containing $[Ru^{II}(Me_2phen)_3]^{2+}$, $Sc(NO_3)_3$ and a heteropolynuclear cyanide metal complex under visible light irradiation with a Xenon lamp using a UV light cut filter ($\lambda > 420$ nm). The amount of produced H_2O_2 was determined by spectroscopic titration with an acidic solution of $[TiO(tpypH_4)]^{4+}$ complex (Ti-TPyP reagent).[25] Among various hetropolynuclear cyanide complexes, $Fe_3[Co(CN)_6]_2$ exhibited the highest catalytic reactivity.

A series of the heteropolynuclear cyanide complexes $(Fe_xCo_{1-x})_3[Co(CN)_6]_2$ (x = 0, 0.10, 0.50, 0.75, 0.90 and 1) were prepared by mixing an aqueous solution of $K_3[Co^{III}(CN)_6]$, $Co^{II}(NO_3)_2$ and $Fe^{II}(ClO_4)_2$ with various Fe/Co ratios of the (Fe_xCo_{1-x}) moiety ranging from 1:0 to 0:1. All of the synthesised complexes were isostructural with Prussian blue as confirmed by powder X-ray diffraction patterns (Fig. S1†). A schematic drawing of the complex is shown in Fig. 2. The contents of Co and Fe ions of each compound were determined by X-ray fluorescence measurements (Table S1†). The size of $(Fe_xCo_{1-x})_3[Co(CN)_6]_2$ particles remain about the same (260-300 nm) irrespective of the Co to Fe ratio as indicated by the DLS measurements (Fig. S2†).

The catalytic reactivity of $(Fe_xCo_{1-x})_3[Co(CN)_6]_2$ with various x values was examined for the production of H_2O_2 from H_2O and O_2 in an O_2-saturated aqueous solution of $[Ru(Me_2phen)_3]^{2+}$ (100 μM), $Sc(NO_3)_3$ (100 mM) and $(Fe_xCo_{1-x})_3[Co(CN)_6]_2$ (1.0 mg) under photoirradiation of visible light with a Xenon lamp using a UV-light cut filter ($\lambda > 420$ nm) at room temperature as shown in Fig. S3†. The initial rate of production of H_2O_2 increased with increasing the Fe to Co ratio in the (Fe_xCo_{1-x}) moiety (Fr_{Fe}) to reach a maximum at $Fr_{Fe} = 0.75$ and then decreased as shown in Fig. 3. The catalytic reactivity of $(Fe_{0.75}Co_{0.25})_3[Co(CN)_6]_2$ (**1**) was 4.5 and

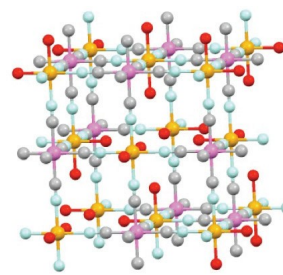**Fig. 2** A schematic drawing of $(Fe_xCo_{1-x})_3[Co(CN)_6]_2$ where x = 0, 0.10, 0.50, 0.75, 0.90 and 1. Ions are colour coded: N-bound Co^{II} and Fe^{II} (orange), C-bound Co^{III} (pink), C (grey), N (blue) and O (red).
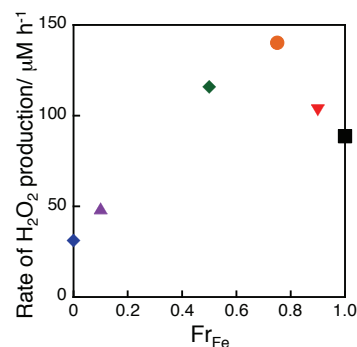

Fig. 3 Initial rates of H_2O_2 production plotted vs. Fr_{Fe}. H_2O_2 was produced from H_2O and O_2 in an O_2-saturated aqueous solution (2.0 mL) of $[Ru(Me_2phen)_3]^{2+}$ (100 μM), $Sc(NO_3)_3$ (100 mM) and $(Fe_xCo_{1-x})_3[Co(CN)_6]_2$ (1.0 mg), where x = 1 (black square), 0.90 (inverse red triangle), 0.75 (orange circle), 0.50 (green diamond), 0.10 (purple triangle) and 0 (blue diamond) under photoirradiation of visible light ($\lambda > 420$ nm) with a Xenon lamp using a UV-light cut filter at room temperature. Time courses of H_2O_2 production are shown in Fig. S3†.

1.5 times enhanced as compared to that of $Co_3[Co(CN)_6]_2$ and $Fe_3[Co(CN)_6]_2$.

The rate of H_2O_2 production was enhanced 2.9 times when N-bound Co ions in $Co_3[Co(CN)_6]_2$ was thoroughly replaced with Fe ions as shown in Fig. 3. Therefore, water oxidation reactivity of N-bound Fe ions was higher than that of N-bound Co ions. On the other hand, the peak attributed to CN ligand stretching observed in IR spectra of $Fe_3[Co(CN)_6]_2$ red shifted as N-bound Fe^{II} ions were replaced with Co^{II} ions (Fig. S4†). This is because an Fe^{II} ion can accept electrons from bonding orbitals of CN ligands rather easily than a Co^{II} ion because of its low LUMO level. The electron-rich CN ligands can stabilise high valence metal ions that form in water oxidation process. Therefore, the volcano-type dependence of rate of H_2O_2 production on Fr_{Fe} is considered to be result of those two contradictory effects of Fr_{Fe} on water oxidation reaction where a complex with a large Fr_{Fe} would contain more active sites for water oxidation while a complex with smaller Fr_{Fe} would easily stabilise high valence metal ions formed during water oxidation.

The catalytic activity of $(Fe_xCo_{1-x})_3[Co(CN)_6]_2$ was also examined in the photocatalytic oxidation of water with persulfate ($Na_2S_2O_8$) using $[Ru(bpy)_3]^{2+}$ (bpy = 2,2'-bipyridine) as a photocatalyst. The photocatalytic cycle is given in Scheme 2, where the excited state of $[Ru(bpy)_3]^{2+}$ was oxidatively quenched by $Na_2S_2O_8$ to produce $[Ru(bpy)_3]^{3+}$, which oxidises water in the presence of $(Fe_xCo_{1-x})_3[Co(CN)_6]_2$ acting as a WOC to evolve O_2. The time courses of
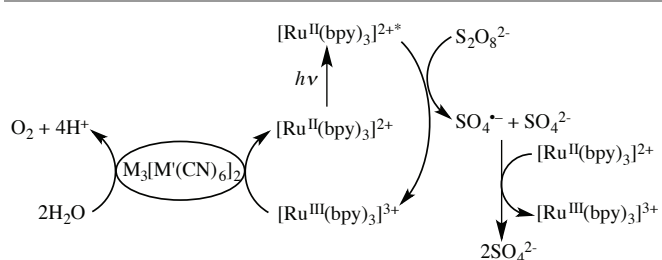
Scheme 2 Photocatalytic cycle of water oxidation with $Na_2S_2O_8$ using $[Ru(bpy)_3]^{2+}$ as a photocatalyst and $(Fe_xCo_{1-x})_3[Co(CN)_6]_2$ as a water oxidation catalyst.
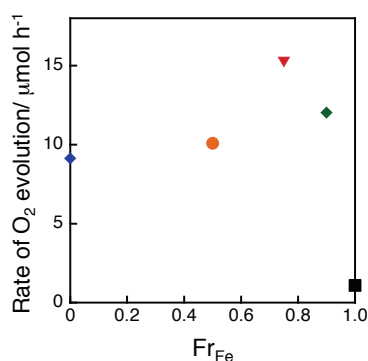

Fig. 4 Initial rate of O_2 evolution plotted versus Fr_{Fe}. O_2 evolution was performed by photoirradiation ($\lambda > 420$ nm) of an aqueous phosphate buffer (2.0 mL) containing $Na_2S_2O_8$ (5.0 mM), $Ru[(bpy)_3]^{2+}$ (100 μM) and $(Fe_xCo_{1-x})_3[Co(CN)_6]_2$ (1.0 mg), where x = 1 (black square), 0.90 (green diamond), 0.75 (red inverse triangle), 0.50 (orange circle) and 0 (blue diamond), at pH 8.0 at room temperature. The time courses of O_2 evolution are shown in Fig. S5†.

O_2 evolution in the photocatalytic water oxidation with $Na_2S_2O_8$ in the presence of $[Ru(bpy)_3]^{2+}$ and $(Fe_xCo_{1-x})_3[Co(CN)_6]_2$ are shown in Fig. S5†. The O_2 evolution rate was maximised at $Fr_{Fe} = 0.75$ which also gave the most effective WOC for photocatalytic H_2O_2 production (Fig. 4). Catalytic O_2 evolution by water oxidation was also confirmed when $[Ru^{III}(Me_2phen)_3]^{3+}$ was added to an aqueous suspension of **1** at pH 3.0, the same pH condition as H_2O_2 production reaction (Fig. S6†).

The dependence of the rate of production of H_2O_2 on the amount of **1** and $[Ru(Me_2phen)_3]^{2+}$ was examined to obtain the optimised conditions where the amount of **1** is 1.0 mg and $[[Ru(Me_2phen)_3]^{2+}]$ = 100 μM (Fig. S7†). Under such optimised conditions, the quantum efficiency with $\lambda = 450$ nm and solar energy conversion efficiency with a solar simulator (HAL-320, Asahi Spectra Co., Ltd.) were determined to be 6.9 % and 0.13 %, respectively (Fig. S8†).[26]

1 was found to maintain its original catalytic activity for at least 5 repetitive photocatalytic production of H_2O_2 (Fig. S9†). There was no significant difference between IR spectra as well as XRD patterns of **1** before the reaction and those of the precipitate obtained after centrifugation of the reaction solution, indicating the robustness of **1** in the reaction conditions (Fig. S10†). DLS data obtained after the reaction (Fig. S10c†) demonstrated no formation of significantly smaller nanoparticles such as metal oxides or hydroxides that could have been *in-situ* formed with wide distribution of the particle size in many other cases of Co and other transition metal-based WOCs as reported previously.[27-31] From the
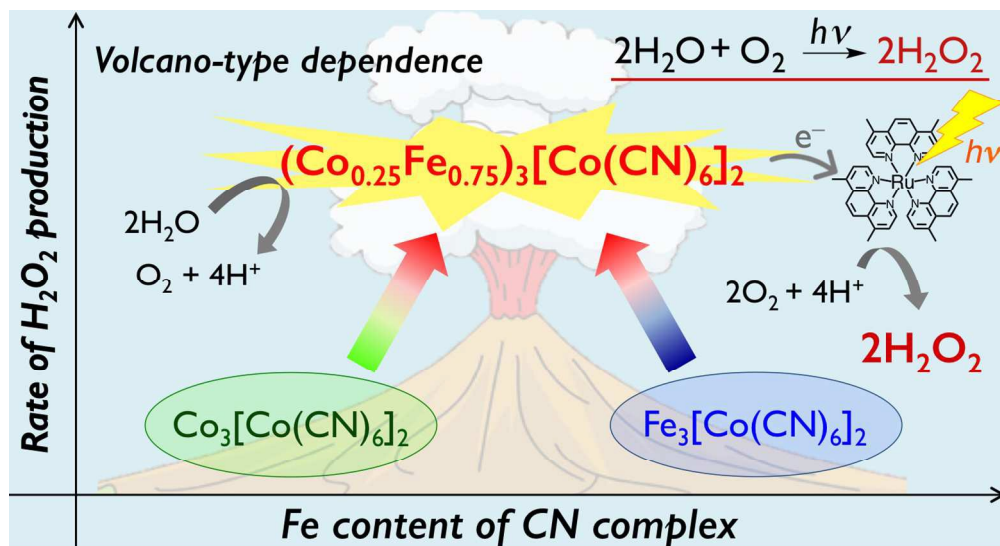
results mentioned above, we can conclude that the actual catalytically active species for water oxidation in H_2O_2 production is **1** as it is.[32]

In conclusion, cyano-bridged polynuclear complexes $(Fe_xCo_{1-x})_3[Co(CN)_6]_2$ act as effective water oxidation catalysts for the photocatalytic oxidation of H_2O with O_2 to produce H_2O_2 in an O_2-saturated aqueous solution in the presence of $[Ru(Me_2phen)_3]^{2+}$ and $Sc(NO_3)_3$ under visible light irradiation. The catalytic activity was maximised when Fe to Co ratio in the (Fe_xCo_{1-x}) moiety of $(Fe_xCo_{1-x})_3[Co(CN)_6]_2$ was 0.75. This study provides a unique way to develop efficient catalysts for the photocatalytic water oxidation with O_2 to produce H_2O_2 by changing the ratio of different metals contained in cyano-bridged polynuclear metal complexes.

Notes and references

1   S. Fukuzumi, Y. Yamada and K. D. Karlin, *Electrochim. Acta*, 2012, **82**, 493-511.
2   S. Fukuzumi, Y. Yamada, *Aust. J. Chem.*, 2014, **67**, 354-364.
3   L. An, T. Zhao, X. Yan, X. Zhou and P. Tan, *Science Bull.*, 2015, **60**, 55-64.
4   S. Yamazaki, Z. Siroma, H. Senoh, T. Ioroi, N. Fujiwara and K. Yasuda, *J. Power Sources*, 2008, **178**, 20-25.
5   Y. Yamada, Y. Fukunishi, S. Yamazaki and S. Fukuzumi, *Chem. Commun.*, 2010, **46**, 7334-7336.
6   Y. Yamada, S. Yoshida, T. Honda and S. Fukuzumi, *Energy Environ. Sci.*, 2011, **4**, 2822-2825.
7   S. A. M. Shaegh, N. T. Nguyen, S. M. M. Ehteshami and S. H. A. Chan, *Energy Environ. Sci.*, 2012, **5**, 8225-8228.
8   Y. Yamada, M. Yoneda and S. Fukuzumi, *Chem.–Eur. J.*, 2013, **19**, 11733-11741.
9   Y. Yamada, M. Yoneda and S. Fukuzumi, *Inorg. Chem.*, 2014, **53**, 1272-1274.
10   F. Yang, K. Cheng, T. Wu, Y. Zhang, J. Yin, G. Wang, and D. Cao, *RSC Adv.*, 2013, **3**, 5483-5490.
11   F. Yang, K. Cheng, X. Xiao, J. Yin, G. Wang and D. Cao, *J. Power Sources*, 2014, **245**, 89-94.
12   X. Xiao, F. Yang, K. Cheng, X. Wang, J. Yin and K. Ye, *J. Electroanal. Chem.*, 2014, **729**, 103-108.
13   Y. Yamada, M. Yoneda and S. Fukuzumi, *Energy Environ. Sci.*, 2015, **8**, 1698-1701.
14   B. Reuillard, S. Gentil, M. Carrière, A. L. Goff and S. Cosnier, *Chem. Sci.*, 2015, **6**, 5139-5143.
15   S. Kato, J. Jung, T. Suenobu and S. Fukuzumi, *Energy Environ. Sci.*, 2013, **6**, 3756-3764.
16   Y. Shiraishi, S. Kanazawa, Y. Kofuji, H. Sakamoto, S. Ichikawa and S. Tanaka, *Angew. Chem.*, *Int. Ed.*, 2014, **53**, 13454-13459.
17   Y. Isaka, S. Kato, D. Hong, T. Suenobu, Y. Yamada and S. Fukuzumi, *J. Mater. Chem. A*, 2015, **3**, 12404-12412.
18   D. Hong, J. Jung, J. Park, Y. Yamada, T. Suenobu, Y. M. Lee, W. Nam and S. Fukuzumi, *Energy Environ. Sci.*, 2012, **5**, 7606-7616.
19   D. Hong, M. Murakami, Y. Yamada and S. Fukuzumi, *Energy Environ. Sci.*, 2012, **5**, 5708-5716.
20   Y. Yamada, K. Oyama, R. Gates and S. Fukuzumi, *Angew. Chem., Int. Ed.*, 2015, **54**, 5613-5617.
21   H. J. Buser, D. Schwarzenbach, W. Petter and A. Ludi, *Inorg. Chem.*, 1977, **16**, 2704-2710.
22   X.-P. Shen, Y.-Z. Li, Y. Song, Z. Xu and G.-C. Guo, *Eur. J. Inorg. Chem.*, 2007, 1698-1702.

23 J. M. Herrera, A. Bachschmidt, F. Villain, A. Bleuzen, V. Marvaud, W. Wernsdorfer and M. Verdaguer, *Philos. Trans. R. Soc., A*, 2008, **366**, 127-138.

24 M. Verdaguer and G. S. Girolami, in *Magnetism: molecules to materials, Vol. V* (Eds.: J. S. Miller, M. Drillon), Wiley-VCH, Weinheim, **2005**.

25 C. Matsubara, N. Kawamoto and K. Takamura, *Analyst*, 1992, **117**, 1781-1784.

26 The light intensity was adjusted at 10 mJ cm^{-2} s^{-1} (Air Mass 1.5 (AM1.5)) at the sample position for whole irradiation area (1.0 × 3.0 cm^2) by 1 SUN checker (CS-20, Asahi Spectra Co., Ltd.) at room temperature.

27 Q. Yin, J. M. Tan, C. Besson, Y. V. Geletii, D. G. Musaev, A. E. Kuznetsov, Z. Luo, K. I. Hardcastle and C. L. Hill, *Science*, 2010, **328**, 342-345.

28 H. Lv, J. Song, Y. V. Geletii, J. W. Vickers, J. M. Sumliner, D. G. Musaev, P. Kögerler, P. F. Zhuk, J. Bacsa, G. Zhu, and C. L. Hill, *J. Am. Chem. Soc.*, 2014, **136**, 9268–9271.

29 J. J. Stracke and R. G. Finke, *ACS Catal.*, 2014, **4**, 79–89.

30 J. J. Stracke and R. G. Finke, *ACS Catal.*, 2014, **4**, 909–933.

31 J. D. Blackmore, R. H. Crabtree and G. W. Brudvig, *Chem. Rev.*, 2015, DOI: 10.1021/acs.chemrev.5b00122.

32 The major reason for the decrease of catalytic activity of the system at prolonged reaction time (Fig. 1) may result from the gradual deactivation of $[Ru^{II}(Me_2phen)_3]^{2+}$, however, no formation of RuO_2 nanoparticles was confirmed by XRD as well as DLS data recorded after the reaction (Fig. S10†).

550x296mm (72 x 72 DPI)